



Cite this: DOI: 10.1039/d2lc00012a

An antibiotic concentration gradient microfluidic device integrating surface-enhanced Raman spectroscopy for multiplex antimicrobial susceptibility testing†

Shang-Jyun Lin,^a Po-Hsuan Chao,^a Ho-Wen Cheng,^{bc} Juen-Kai Wang,^{bde} Yuh-Lin Wang,^{ID d} Yin-Yi Han^{fg} and Nien-Tsu Huang ^{ID *ah}

Antimicrobial susceptibility testing (AST) is a key measure in clinical microbiology laboratories to enable appropriate antimicrobial administration. During an AST, the determination of the minimum inhibitory concentration (MIC) is an important step in which the bacterial responses to an antibiotic at a series of concentrations obtained in separate bacterial growth chambers or sites are compared. However, the preparation of different antibiotic concentrations is time-consuming and labor-intensive. In this paper, we present a microfluidic device that generates a concentration gradient for antibiotics that is produced by diffusion in the laminar flow regime along a series of lateral microwells to encapsulate bacteria for antibiotic treatment. All the AST preparation steps (including bacterium loading, antibiotic concentration generation, buffer washing, and isolated bacterial growth with an antibiotic) can be performed in a single chip. The viable bacterial cells in each microwell after the antibiotic treatment are then quantified by their surface-enhanced Raman scattering (SERS) signals that are acquired after placing a uniform SERS-active substrate in contact with all the microwells. For proof-of-concept, we demonstrated the AST performance of this system on ampicillin (AMP)-susceptible and -resistant *E. coli* strains. Compared with the parameters for conventional AST methods, the AST procedure based on this chip requires only 20 µL of bacteria solution and 5 h of operation time. This result indicates that this integrated system can greatly shorten and simplify the tedious and labor-intensive procedures required for current standard AST methods.

Received 6th January 2022,
Accepted 17th March 2022

DOI: 10.1039/d2lc00012a

rsc.li/loc

Introduction

Due to the misuse and over-consumption of antibiotics, antimicrobial-resistant (AMR) bacteria have become a serious issue that makes the medical treatment of bloodstream

infections (BSIs) and urinary tract infections (UTIs) difficult.^{1–3} Antimicrobial susceptibility testing (AST) is a standard laboratory procedure that evaluates the antibiotic resistance of bacteria by measuring the susceptibility of bacteria to antibiotics. To perform an AST, bacteria are first treated with a wide range of antibiotic concentrations. The minimum inhibitory concentration (MIC) is then determined based on the growth pattern. Although conventional phenotype AST methods, such as disk diffusion and broth microdilution (BMD), are widely applied in laboratories and hospitals, the required sample preparation procedures are usually time-consuming and labor-intensive.^{4,5} In addition, bacterial morphological responses to specific antibiotics, such as elongation and filamentation, may be mistaken as bacterial growth.^{6,7} Although culture-free methods, such as nucleic acid amplification technologies (NAATs), have been developed for AST to address this issue,^{8,9} it still suffers several problems. First, nucleic acid amplification-based methods cannot differentiate viable and unviable DNAs.¹⁰ Second, whole blood compositions, such as anticoagulants, iron, immunoglobulins, and lactoferrin, may inhibit the

^a Graduate Institute of Biomedical Electronics and Bioinformatics, National Taiwan University, Taipei, Taiwan. E-mail: nthuang@ntu.edu.tw

^b Institute of Atomic and Molecular Sciences, Academia Sinica, Taipei, Taiwan

^c International Graduate Program of Molecular Science and Technology, National Taiwan University (NTU-MST) and Taiwan International Graduate Program (TIGP), Academia Sinica, Taipei, Taiwan

^d Center for Condensed Matter Sciences, National Taiwan University, Taipei, Taiwan

^e Center for Atomic Initiative for New Materials, National Taiwan University, Taipei, Taiwan

^f Department of Anesthesiology, National Taiwan University Hospital, Taipei, Taiwan

^g Department of Trauma, National Taiwan University Hospital, Taipei, Taiwan

^h Department of Electrical Engineering, National Taiwan University, Taipei, Taiwan

† Electronic supplementary information (ESI) available. See DOI: 10.1039/d2lc00012a

PCR.¹¹ Lastly, healthy donors or patients after successful treatment may still have bacterial DNA or RNA, leading to false positive results. Therefore, a new AST method that can detect the physiological activity of bacteria, rather than their phenological appearance or genetic makeup, is urgently needed. We have recently demonstrated a new AST method that exploits released purines and their derivatives detected by surface-enhanced Raman scattering (SERS) to reflect the number of viable cells under the treatment of a series of antibiotic concentrations.¹² The threshold SERS signal of defining the susceptibility to a specific antibiotic can be found via classification analysis.¹³ The resultant AST success rate was higher than 90%, the MIC was determined, and the whole AST protocol can be completed in 5 h. Expediting this manually operated procedure represents an area for improvement. One possible solution is the use of microfluidic technology.

Microfluidic platforms have recently been utilized for bacterial analysis owing to their speed, high throughput, and small footprint. Various studies demonstrated microfluidic microchamber platforms for AST and MIC determination. Although a microchamber can increase the number of sensing spots and reduce the required sample volume and assay time, it is a challenge to simultaneously generate multiple antibiotic concentrations for MIC determination in a single chip. The first method involves fabricating a series of parallel microchannels and introducing different antibiotic concentrations through different inlets^{14,15} or the same antibiotic concentration into different microchamber sizes.¹⁶ Another method is based on the laminar flow behavior of microfluidics. A concentration gradient generator (CGG) can be built with a Christmas tree-shaped microchannel, whereas two samples introduced into two inlets merge, mix, separate, and repeatedly dilute to generate a stable concentration gradient at the outlets.^{17–19} The drawback of this design is the complex and large channel geometry.¹⁹ One alternative design is based on laminar flow plus diffusion phenomena. In this design, two samples are introduced into a Y-shaped main channel with a series of side channels.^{20–23} The laminar flow that occurs in the main channel generates an antibiotic concentration gradient from upstream to downstream. Based on the diffusion behavior, the side channel along the main channel experiences different antibiotic concentrations.^{24–26} Although this design was previously demonstrated for MIC determination, issues still exist. First, the above methods usually use imaging-based methods, such as bacteria counting or fluorescence labeling, to quantify the effect of antibiotics on the bacteria.²⁷ These results may be misinterpreted due to bacteria aggregation or elongation behavior. Another indirect method to quantify bacteria AST response is the use of resazurin. Since living bacteria reduce non-fluorescent resazurin (blue) to fluorescent resorufin (pink), the bacteria amount or AST results can be quantified by measuring the fluorescence intensity. Detection methods based on fluorescent agents suffer several drawbacks (including a short lifetime and errors in calibrating the

emitted signal and in counting the aggregated cells) that may result in incorrect results. In addition to the above methods, surface-enhanced Raman spectroscopy (SERS) is also widely applied for bacteria identification or ASTs.^{12,13,28,29} Since the bacterial SERS signal originates from its released purines and their derivatives,^{30,31} it possesses several advantages: (1) it is label-free, (2) it is non-invasive and (3) it reflects physiological activity. These advantages favor the integration of a SERS-based detection method with a multiplex microfluidic platform for high-throughput AST if the performance of the SERS-active substrate is uniform and reliable.

In this paper, we report an antibiotic concentration gradient microfluidic (ACGM) device that integrates a SERS substrate that performs multiplex AST. The antibiotic concentration gradient is generated by mixing a high-concentration antibiotic solution and pure medium through a main channel. Then, the concentration level varies along the main channel, and the solution diffuses into each side channel. In each side channel, a microwell array unit is placed underneath enabling bacteria encapsulation while the antibiotic concentration is being generated, medium washing, and the isolation process. Once the above procedures are done, the main channel layer is replaced by the SERS substrate for large-area SERS mapping measurement. By synchronizing the motorized stage and SERS spectrometer, the SERS signal of 792 microwells can be automatically scanned in 70 min. This comprehensive SERS profile can provide rich information for AST and MIC determination in a single chip. For proof of concept, we loaded ampicillin (AMP)-susceptible and -resistant *Escherichia coli* (*E. coli*) strains into the ACGM device and performed *in situ* SERS mapping to determine the MIC value for the susceptible *E. coli* strain. In summary, all the required sample preparation processes, including bacteria encapsulation, antibiotic concentration generation, washing, isolation, and *in situ* SERS measurement, can all be done in a single device.

Materials and methods

Bacterial sample preparation

E. coli (BW25113) was purchased from the American Type Culture Collection (ATCC) and served as the AMP-susceptible strain. The *E. coli* (DH5α AMP^r) purchased from Yeastern Biotech Co. Ltd. was transformed with a pGS-21 plasmid for AMP resistance and served as the resistant strain. AMP was purchased from Sigma-Aldrich. All the bacteria samples were cultured in a Mueller Hinton broth (MHB) that was purchased from BD Biosciences. The bacteria were resolubilized with a 5 mL culture medium and incubated at 37 °C and 200 rpm for 16–18 h. Next, 0.2 mL of the overnight-cultured sample was added to another 5 mL MHB and incubated for 2 h to reach an exponential phase. Then, the cultured bacteria sample was adjusted to 10⁸ CFU mL⁻¹ based

on its optical density ($OD_{600} = 0.5$) before loading it into the ACGM device.

The ACGM device and SERS substrate fabrication

Both layers of the ACGM device were made of polydimethylsiloxane (PDMS) (Sylgard-184, Dow Corning) based on a standard soft lithography process,²⁹ aligned with a stereoscope (SZ61TR, Olympus), and temporarily bonded together based on the electrostatic force. The SERS substrate was fabricated by following our previous protocol.³² Briefly, the glass slide was first pre-cleaned with acetone and hydrofluoric acid. Then, a silver film with an average thickness of 7 nm was deposited with an electron beam evaporator (EBS-300, Junsun Tech) with an evaporation rate of 0.3 nm min⁻¹.

SERS measurement and spectral processing

The SERS spectra were collected using a standard epifluorescence microscope (BX61WI, Olympus) equipped with a Raman fiber probe sensor (SuperHead HE 640, Horiba) and a spectrometer (HE 633, Horiba). The light source was a 632.8 nm He–Ne laser (LGK 7665 P18, LASOS). All SERS measurements were conducted using a 20× objective lens (MPlanFL N, Olympus, and laser spot size of ~25 μm) with 5 mW laser irradiation power. The SERS signal was dispersed using an 80 cm spectrograph (1200 gr mm⁻¹) and detected with a thermoelectric-cooled charge-coupled device (CCD) (354308, Horiba). The calibrated spectral resolution and error were 4 and 0.1 cm⁻¹, respectively. The device was raster-scanned with a motorized stage (EK32 75 × 50, Märzhäuser). Each SERS spectrum was an average of 3 repeated cycles. The background removal of the SERS spectrum was processed based on the sensitive nonlinear iterative peak clipping algorithm proposed by Matoušek's group.³³ To simplify the SERS mapping results among the 792 microwells, we calculated the Raman peak intensity within the 733 ± 10 cm⁻¹ range (I_{733}) and defined it as the pixel intensity of the microwells to form the SERS heatmap.

Bright-field and fluorescence optical imaging setup

To quantify the particle trapping efficiency and subsequent washing efficiency, we captured fluorescence images with an inverted fluorescence microscope (IX-73, Olympus) equipped with a dual-color CCD camera (DP-80, Olympus) using a 20× (PlanN, Olympus) objective lens. Stitching images were composed using a microscopy analysis software (CellSens, Olympus). To quantify the fluorescence intensity or fluorescent bead numbers for each microwell, a fixed circle size was selected, and all the pixel intensities or bead numbers inside the circle were calculated by ImageJ software (Fiji 1.52p). Since the whole measurement range was quite large (11 mm × 32.2 mm), we placed the ACGM device on a customized rotation stage to ensure that the scanning direction was parallel to the main channel direction.

Results and discussion

The ACGM device design

A schematic of the ACGM device is shown in Fig. 1A. It was composed of (1) a top layer that consisted of a Y-shaped main channel with 66 side channels that can generate an antibiotic concentration gradient in each side channel based on the laminar flow and diffusion behavior that occurred in the main channel and (2) a bottom layer that consisted of 66 microwell array units. In each unit, there were 12 individual microwells placed underneath each side channel. Once the bottom microwell array was filled with antibiotic-treated bacteria samples, the top main channel layer was replaced by the SERS substrate for *in situ* SERS measurements (Fig. 1B). The length (L) and width (W) of the main channel and side channel were 20 mm and 300 μm and 1 mm and 300 μm, respectively. The diameter (D) and height (H) of a single microwell were 100 μm and 150 μm, respectively. To generate an antibiotic concentration gradient, the antibiotic mixed MHB and pure MHB solutions were simultaneously introduced into the Y-shaped main channel using a syringe pump (Fusion 100, Chemex Inc.). To achieve an optimal mixing behavior of the two solutions, the angle and the length of the Y-shaped inlets were designed and optimized based on previous research.²⁰ To ensure that the high or low SERS signal was not due to lack of antibiotic exposure (high SERS signal) or unfavorable bacterial growth (low SERS signal), negative (channel #0) and positive (channel #65) control side channels were placed before the mixing behavior occurred. To mimic the antibiotic concentration gradient profile, we simultaneously introduced red and blue food dyes into the ACGM device, as shown in Fig. 1C. Fig. 1D shows a photograph of the bottom microwell array layer that was attached to the SERS substrate for SERS measurement.

The multiplex SERS-AST protocol operated by the ACGM device

The multiplex SERS-AST protocol operated by the ACGM device is shown in Fig. 2. First, the bacterial solution at a concentration of 10^8 CFU mL⁻¹ was manually loaded into the device from both inlets using pipette tips to fill the main channel, side channel, and microwells underneath. After a 10–15 min loading time, the bacteria were encapsulated inside the microwell arrays (step 1). To remove any bubble remaining in the channel, the ACGM device was first placed in a vacuum chamber for 30 min. In this treatment, the air bubbles in the side channel disappeared in 5 min after the bacteria loading process. Next, high-concentration antibiotics in the MHB (purple) and pure MHB (yellow) were introduced into the ACGM device individually from two inlets at a rate of 0.4 μL min⁻¹ to generate the antibiotic concentration gradient (step 2). It took approximately 50 min to obtain a stable concentration gradient in each side channel. Then, air was introduced from the outlet to isolate each side channel (step 3). This step produced an isolated antibiotic concentration microenvironment in each side channel for bacteria incubation. To prevent evaporation, the ACGM device was placed inside a Petri dish with DI water droplets nearby to keep a high humidity environment during incubation. After incubation for 3 h, DI water

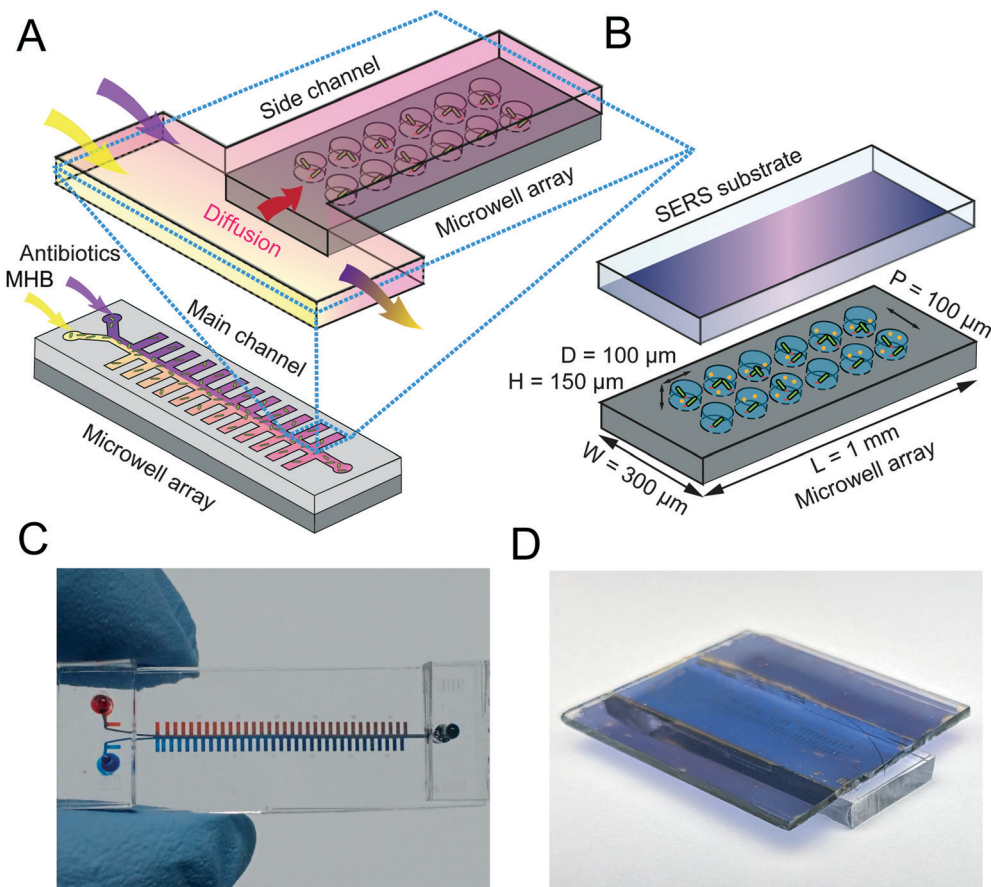


Fig. 1 (A) Schematic of the ACGM device. The blue-framed inset shows the detailed microwell array and antibiotic concentration layout. (B) Schematic of the microwell array detached from the top main channel layer and attached to the SERS substrate for *in situ* SERS measurement. The dimensions of the single side channel and microwell unit were 1 mm (L) \times $300\text{ }\mu\text{m}$ (W) and $100\text{ }\mu\text{m}$ (D) \times $150\text{ }\mu\text{m}$ (H), respectively. (C) Photograph of the ACGM device introduced with red and blue dyes to mimic the concentration gradient profile. (D) Photograph of the bottom microwell array layer attached to the SERS substrate for SERS measurement.

was introduced from the outlet to wash out the bacteria broth inside the side channel and microwells (step 4). This step can minimize the background Raman signal interference from the medium and further stimulate the bacteria to secrete more metabolites in a nutrient insufficient environment. Next, the second air isolation step was performed (step 5). Then, the top main channel was gently peeled off, which allowed each microwell to be filled with the solution based on the surface tension (step 6). Finally, the bottom microwell layer was covered by the SERS substrate for SERS measurement (step 7). The reason for using 10^8 CFU mL^{-1} as the initial bacteria concentration is that some bacteria inside the ACGM device (step 1, Fig. 2) may be flushed out during the antibiotic concentration gradient generation process (step 2, Fig. 2). Based on the microscopy images, we found that the equivalent bacteria concentration is around $2.5\text{--}5 \times 10^7\text{ CFU mL}^{-1}$, which is similar to the bacteria concentration we used in our previous SERS-AST experiments.^{13,34}

Concentration gradient generation

To determine the ideal injection rate for the two samples to generate a uniform concentration gradient (step 2 in Fig. 2), we

used commercial finite element method (FEM) software (COMSOL 5.5, Multiphysics) to simulate the concentration distribution at three flow rates (0.2 , 0.4 , and $0.6\text{ }\mu\text{L min}^{-1}$). The diffusion coefficient of AMP was set as $400\text{ }\mu\text{m}^2\text{ s}^{-1}$.³⁵ The normalized concentration profile of the ACGM device is shown in Fig. S1A.† To further compare the concentration level change, the normalized concentration at each side channel was averaged and is plotted in Fig. S1B.† Based on the simulation results, we chose $0.4\text{ }\mu\text{L min}^{-1}$ as the injection flow rate since the concentration change along channels #1 to #32 is more linear and distinct compared to the other two flow rates, which can better identify the interesting antibiotic concentration level in this region. Another reason is that, due to a high flow resistance in the ACGM device, the flow pattern at $0.4\text{ }\mu\text{L min}^{-1}$ is relatively stable compared to the case at $0.2\text{ }\mu\text{L min}^{-1}$. Next, we used fluorescein isothiocyanate (FITC) as a phantom to evaluate the concentration gradient profile in the ACGM device since its molecular weight ($\text{MW} = 389.38\text{ g mol}^{-1}$) is similar to that of AMP ($\text{MW} = 349.41\text{ g mol}^{-1}$). Here, we introduced 1 mg mL^{-1} FITC solution and pure water from two inlets and followed the SERS-AST protocol to generate a concentration gradient (step 2 in Fig. 2); this was followed by 1st air isolation (side channel isolation) (step 3 in

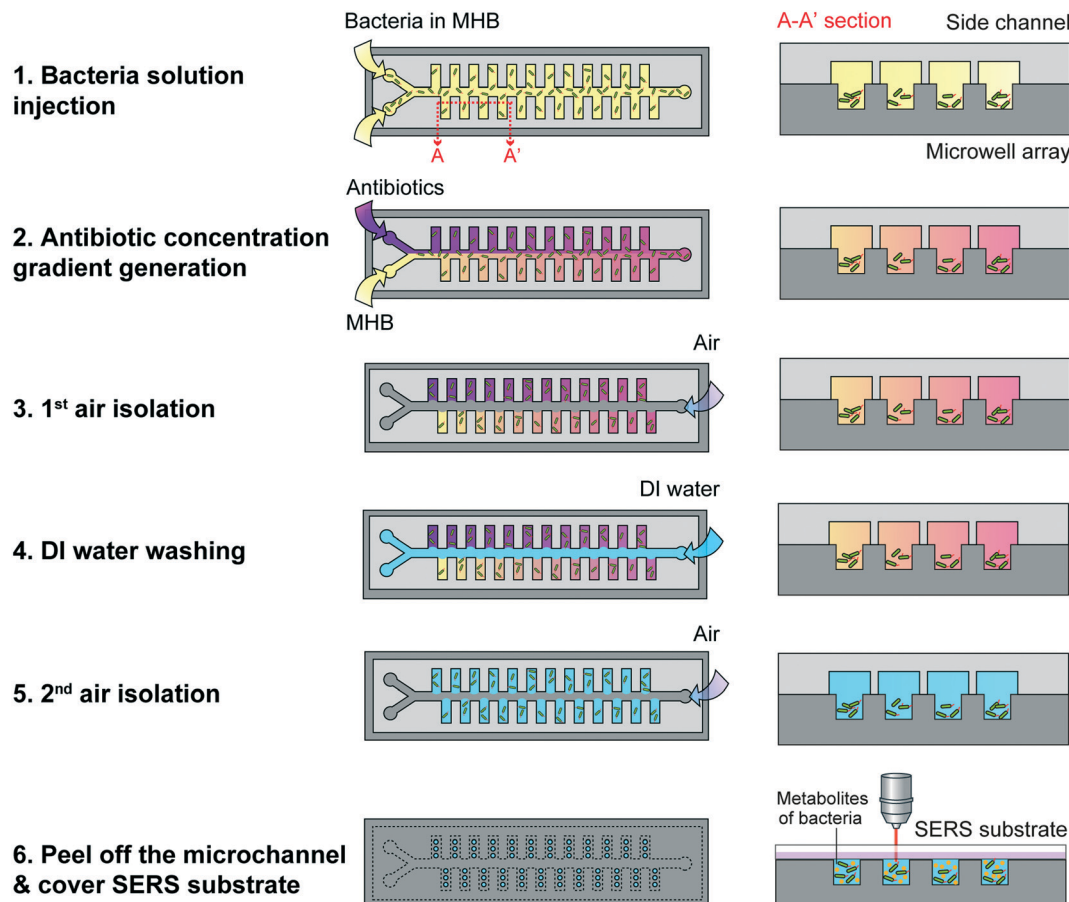


Fig. 2 The multiplex SERS-AST protocol conducted with the ACGM device. The protocol includes (1) bacteria solution injection into both inlets, (2) antibiotic concentration gradient generation by loading the antibiotic in the MHB (purple) and pure MHB (yellow) individually into two inlets at $0.4 \mu\text{L min}^{-1}$, (3) 1st air isolation by introducing air from the outlet to isolate each side channel and perform bacteria treatment at various antibiotic concentrations for 3 h, (4) DI water washing to wash out the bacteria broth inside the side channel and microwells, (5) 2nd air isolation by introducing air from the outlet to isolate each side channel and allow the bacteria to secrete metabolites in a nutrient insufficient environment, and (6) the top microchannel layer being replaced by a SERS substrate for SERS measurement.

Fig. 2) and 2nd air isolation (microwell isolation) processes (step 5 in Fig. 2). The fluorescence images of the three steps are shown in Fig. 3A. To further evaluate the fluorescence intensity inside the microwells, the inset image for channel #32 (orange-framed image) was magnified. As shown in the inset image, an extremely low fluorescence intensity was distributed outside the microwell in the last step, indicating successful microwell isolation. For the inter-device reproducibility test, we did triplicate experiments using different ACGM devices. By averaging the fluorescence intensity for the 12 microwells in each side channel, the fluorescence intensity profiles of step 3 of the three independent experiments are plotted in Fig. 3B. Although the signal is a little varied among the three experiments at the upper channel region, such signal fluctuation can be compromised since the AST and MIC results were mainly evaluated by the SERS mapping profile at the lower channel region.

Reagent exchange and particle encapsulation efficacy in the DI water washing step

Next, the DI water washing efficiency (step 4 in Fig. 2) was evaluated. There are two parameters to determine the

washing efficiency: (1) the antibiotic exchange rate by DI water and (2) the particle encapsulation rate inside the microwells before and after the washing step. For the first parameter, we used the FITC solution to simulate the antibiotic solution. As shown in Fig. 4A, an FITC concentration gradient was generated. Then, DI water was introduced from the outlet at $5 \mu\text{L min}^{-1}$. At each time point (0, 5, 10, 15, 20, and 25 min), the fluorescence intensity of the ACGM device was recorded. To evaluate the washing efficiency in different channel regions, we selected the red (channel #63), blue (channel #48), and green (channel #34) channels as the representative channels for the upstream, midstream, and downstream regions, respectively (Fig. 4B). The corresponding fluorescence intensity of each side channel is shown in Fig. 4C. In all three regions, after 10 min of the washing process, the fluorescence intensity decreased rapidly. After 20 min, the intensity of all the side channels was less than 2% of the highest fluorescence intensity (channel #64 at 0 min), indicating that nearly no FITC was left in the side channels. Then, we used these flow conditions ($5 \mu\text{L min}^{-1}$ for 20 min) to evaluate the particle encapsulation

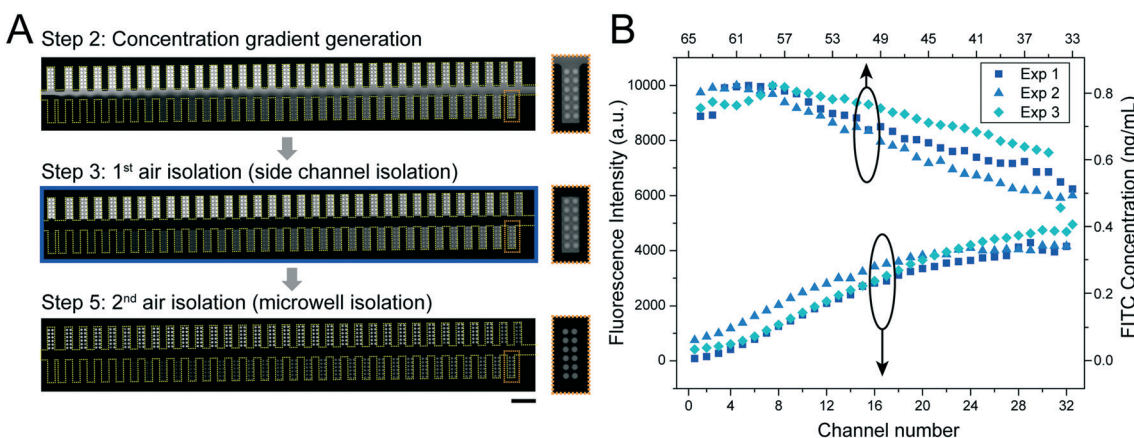


Fig. 3 The concentration gradient generation, side channel, and microwell isolation evaluation in the ACGM device. (A) Fluorescence images with FITC in the microchannel during (1) concentration gradient generation (step 2 in Fig. 2), (2) channel isolation (step 3 in Fig. 2) and (3) microwell isolation (step 5 in Fig. 2). Scale bar: 1 mm. The orange-framed inset shows the magnified image of channel #32. (B) The fluorescence intensity profiles of step 3 of the three independent experiments.

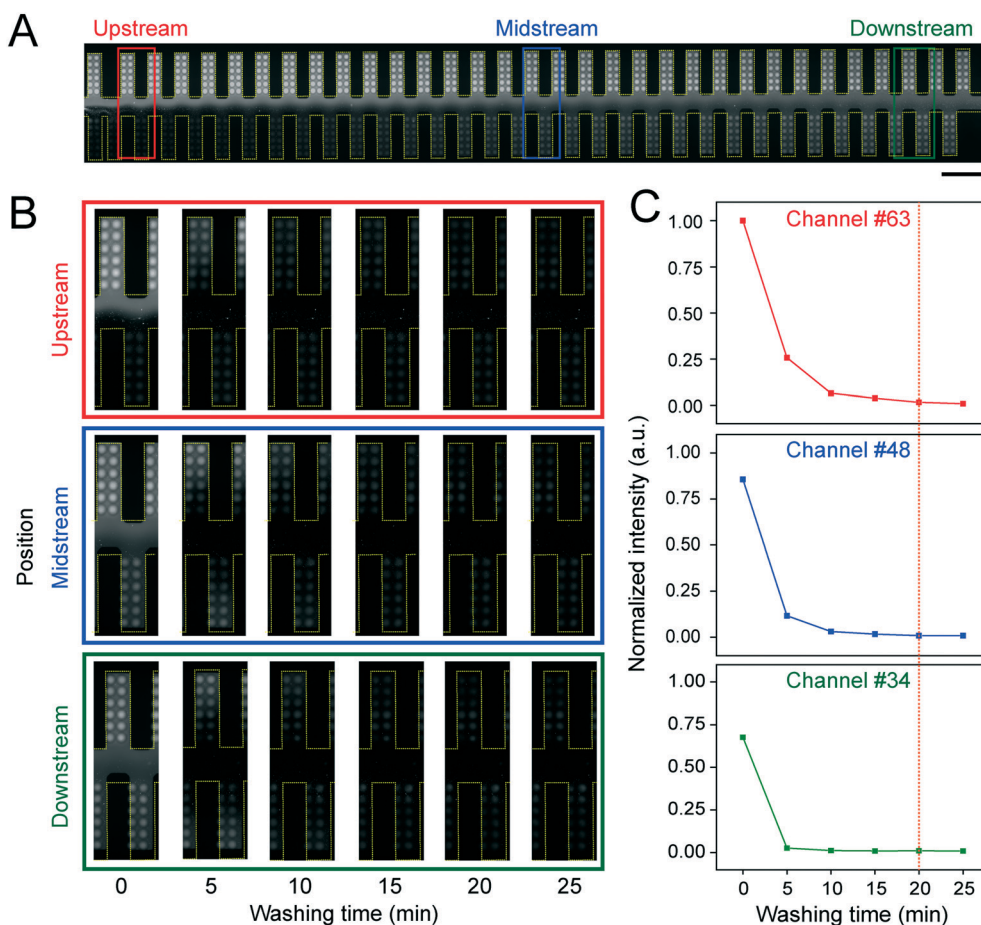


Fig. 4 Washing efficiency evaluation of the ACGM device. (A) Fluorescence image of the complete ACGM device. The red, blue, and green boxes represent the upstream, midstream, and downstream sections, respectively. Scale bar: 1 mm. (B) The fluorescence image of the three sections for 0, 5, 10, 15, 20, and 25 min washing times. (C) The fluorescence intensity of the selected channels (channels #63, #48, and #34) in each section. The washing efficiency was quantified by the normalized fluorescence intensity.

rate before and after the washing step. To mimic the bacteria, we used 2 μ m Fluoresbrite Polychromatic Red microspheres (19508-2, Polysciences) at a concentration of 10^8 beads per

mL and flowed the microspheres into the ACGM device. The bead distribution profiles before and after the washing step are shown in Fig. 5A. The enlarged images of channels #11

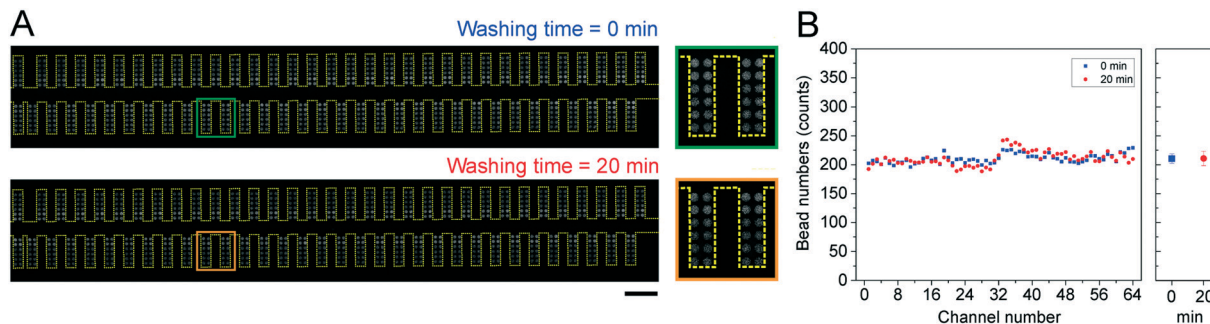


Fig. 5 Bead encapsulation by the microwell arrays during the washing step. (A) Fluorescence images of the ACGM device before and after the washing step (washing time = 0 and 20 min). Scale bar: 1 mm. The blue- and red-framed insets show the magnified images of channels #11 and #12 before (blue) and after (red) the washing step. (B) The calculated bead numbers in the 12 microwells in each channel before (blue) and after (red) the washing step.

and #12 are shown to confirm that all the beads were encapsulated inside the microwells. Based on the bead distribution profiles, the average bead number in each microwell before and after the 20 min washing time was 210.5 ± 7.9 and 210.5 ± 12.4 , respectively. The two numbers are statistically indifferent, indicating that almost all the particles can be still encapsulated inside the microwell during the washing step.

Spatial signal uniformity evaluation of the SERS substrate

Since the main objective of this ACGM device is to perform multiplex SERS-AST in a single chip, it is important to ensure that the SERS signals at different spots are homogenous with a minimum signal variation. To verify the signal variation in the whole sensing area, we flowed 10^{-4} M adenine solution into the ACGM device and measured the corresponding SERS signal at each microwell. The SERS heatmap for the 10^{-4} M adenine is shown in Fig. 6A. Each side channel is composed of 12 pixels, and each pixel intensity represents I_{733} , the

characteristic Raman peak of adenine. To compare the signal differences, the I_{733} values for 12 microwells at each channel were averaged and are plotted in Fig. 6B. The average I_{733} value for all microwells was $23\,205 \pm 1870$ with a coefficient of variation of 8%. To further compare the signal variance in different regions of the device, we selected channel #63 (red, upstream), channel #48 (blue, midstream), and channel #34 (green, downstream) as the representative channels. As shown in Fig. 6C, the SERS spectra for the three channels were quite uniform. Overall, the above results indicate that the large-area SERS mapping measurement in the ACGM device for multiplex SERS-AST is feasible.

Multiplex SERS-AST

Finally, we demonstrated multiplex SERS-AST and MIC determination in the ACGM device using AMP-susceptible (BW25113) and -resistant (DH5 α AMP r) *E. coli* strains at a concentration of 10^8 CFU mL $^{-1}$. First, $64 \mu\text{g mL}^{-1}$ AMP and pure MHB were simultaneously introduced into two inlets at

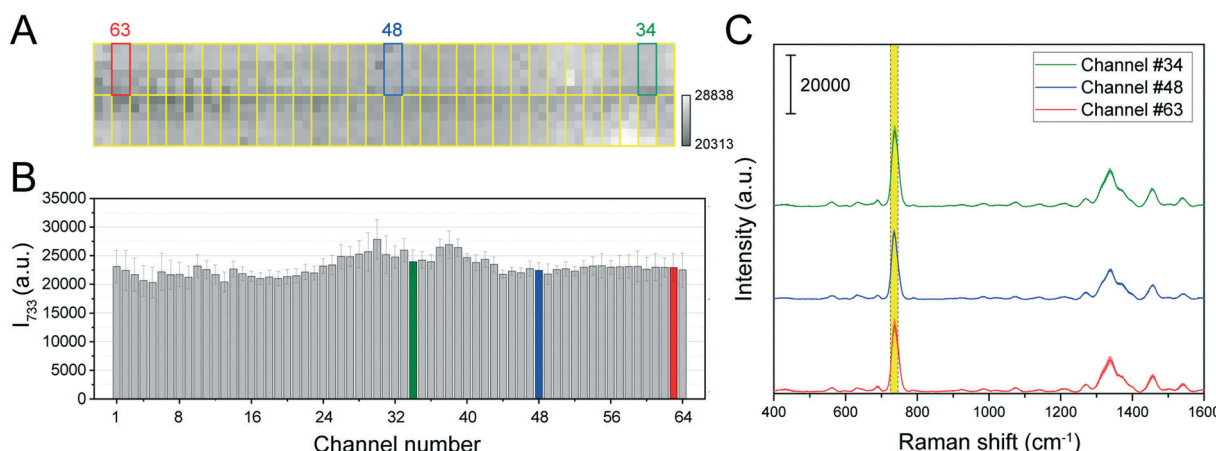


Fig. 6 Spatial signal uniformity evaluation for the SERS substrate using adenine. (A) The SERS heatmap for 10^{-4} M adenine in the ACGM device. (B) The peak intensity at 733 cm^{-1} (I_{733}) for each channel. The red (channel #63), blue (channel #48), and green (channel #34) channels were selected as the representative channels for the upstream, midstream, and downstream sections, respectively. (C) The average SERS spectra for channels #34, #48, and #63.

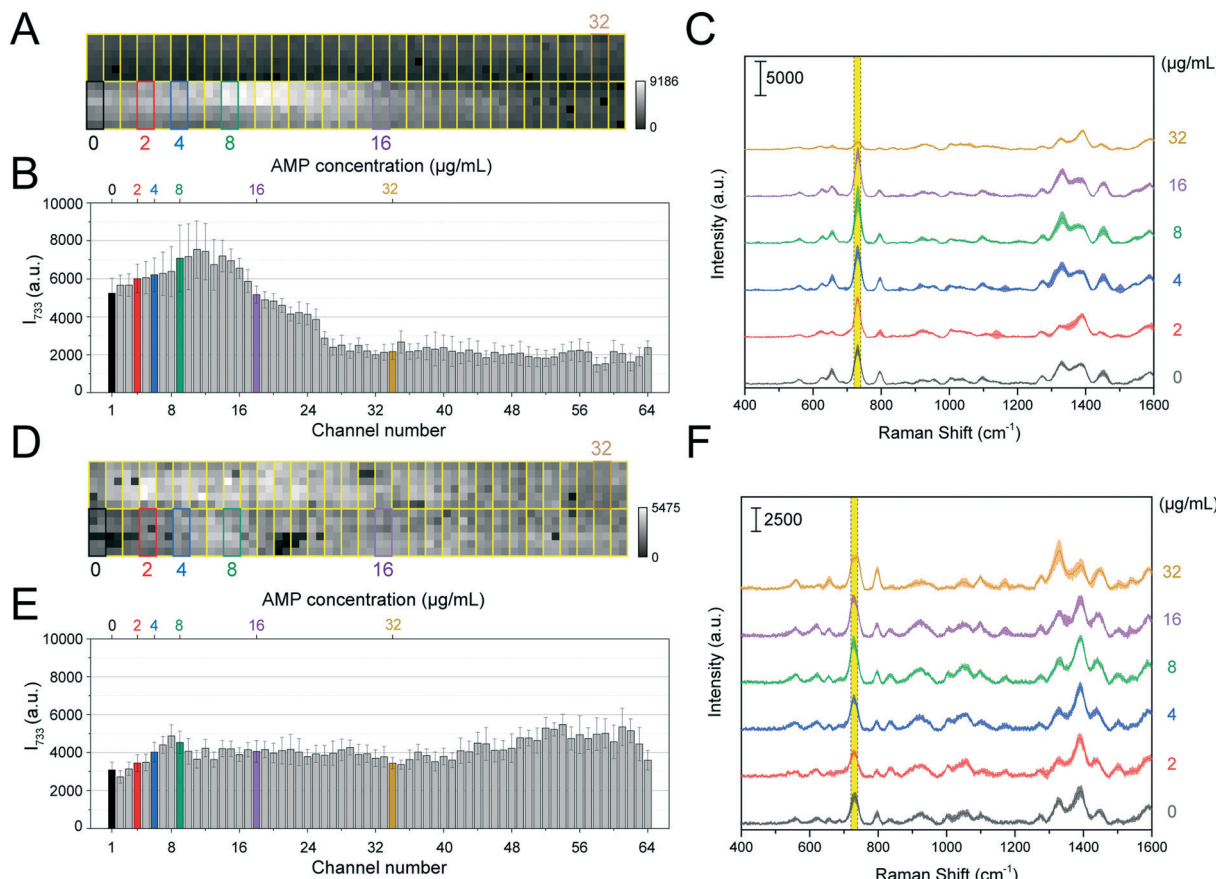


Fig. 7 The multiplex SERS-AST results for (A–C) AMP-susceptible and (D–F) AMP-resistant *E. coli* strains. The SERS heatmap for (A) AMP-susceptible and (D) AMP-resistant *E. coli* strains for AMP concentration gradients from 0 to 32 $\mu\text{g mL}^{-1}$. I_{733} values for (B) AMP-susceptible and (E) AMP-resistant *E. coli* strains among all channels. The top and bottom x-axes represent the AMP concentration and channel number, respectively. The average SERS spectra for the (C) AMP-susceptible and (F) AMP-resistant *E. coli* strains treated with 0, 2, 4, 8, 16, and 32 $\mu\text{g mL}^{-1}$ AMP.

a rate of 0.4 $\mu\text{L min}^{-1}$ to generate an antibiotic concentration gradient. The multiplex SERS-AST results for the AMP-susceptible and -resistant *E. coli* strains are shown in Fig. 7A–C and D–F, respectively. The I_{733} values for the AMP-susceptible (Fig. 7A) and -resistant *E. coli* strains (Fig. 7D) in all microwells were calculated and rearranged as a SERS heatmap. The I_{733} values for the two strains in 12 microwells at each channel were averaged and are plotted in Fig. 7B and E. Based on the previously determined fluorescence concentration gradient profiles (Fig. 3B), the specific antibiotic concentrations at each channel were calculated and labeled for specific side channels (0, 2, 4, 8, 16, and 32 $\mu\text{g mL}^{-1}$ for channels #1, #4, #6, #9, #18, and #34, respectively). The average SERS spectra for the two strains at these representative channels are plotted in Fig. 7C and F. For the AMP-resistant strain, the SERS mapping result showed that the I_{733} values for all side channels were similar, showing no inhibition and indicating that the MIC value of this resistant strain was higher than 64 $\mu\text{g mL}^{-1}$. For the AMP-susceptible strain, at the upper channel region, the I_{733} values for all side channels (channels #32 to #64) were around 2000, which were relatively low due to bacteria

inhibition. Instead, at the lower channel region, the I_{733} value was much higher, indicating that the bacteria can still grow at this antibiotic concentration level. Based on the significant signal difference between channels #25 and #26 (25% intensity drop) shown in Fig. 7B, we defined the MIC value of this strain as approximately 20 $\mu\text{g mL}^{-1}$ (channel #26). For comparison, we conducted a standard BMD method (Fig. S2A†). Both AMP-susceptible and -resistant strains at 5×10^5 CFU mL^{-1} were treated with AMP at various concentrations (0–256 $\mu\text{g mL}^{-1}$) and then incubated overnight at 37 °C. Fig. S2B and C† show the OD values of both strains calculated at each AMP concentration. Based on the results, 16 $\mu\text{g mL}^{-1}$ was determined as the MIC of AMP for the susceptible strain, whereas the OD value remained constant in the resistant strain, even at 256 $\mu\text{g mL}^{-1}$. It is worth mentioning that the way to determine the MIC value may not be exactly the same as the conventional AST method that only uses the antibiotic level in the power of two. Instead, by using this comprehensive SERS mapping profile, we can obtain a more complete bacteria response under different antibiotic concentration level treatments and evaluate the AST response or MIC value more precisely. Another interesting finding is

that for the AMP concentrations from 8–16 $\mu\text{g mL}^{-1}$, the I_{733} values were even higher than those for the concentrations of <8 $\mu\text{g mL}^{-1}$. A possible reason may be due to the hormesis effect. This stimulatory effect was caused by a low dosage of potentially toxic agents.³⁶ A similar response was also observed in our previous study.³⁴ However, by using the ACGM device, we can better quantify this hormesis effect based on a continuous antibiotic concentration gradient.

Conclusions

Herein, we proposed a multiplex SERS-AST assay using an ACGM device that integrates a SERS substrate. Because of its continuous antibiotic concentration gradient, a comprehensive bacteria response to different antibiotic concentrations can be evaluated in a single chip. Overall, three important features were demonstrated. First, we designed a Y-shaped main channel with a series of side channels to create 64 isolated microenvironments for bacteria encapsulation and antibiotic treatment. Compared to the previous on-chip gradient generation design, the microwell array placed underneath each side channel enables multiparallel analysis. Second, the microwell array can successfully confine encapsulated bacteria during multiple sample preparation steps, including antibiotic concentration generation, washing, and isolation steps. Third, high-throughput and multiplex SERS-AST can be realized by a large-area SERS mapping measurement. To further expand the applications of this ACGM device, the overall operation time should be further minimized. One approach is to integrate the bacteria enrichment processes, such as using an acoustic force, to increase the bacteria concentration and decrease the required inoculum time. Furthermore, other potential multiplex analysis besides SERS measurement can also be implemented by replacing the SERS substrate. To summarize, owing to the continuous antibiotic concentration gradient feature, a comprehensive multiplex AST result allows us to better distinguish different bacteria strains, determine MIC values or even study the hormesis effect. Such rich information can be further integrated with machine learning models to study more complicated samples or AST conditions, such as the incubation of multiple bacteria strains or various antibiotic mixture treatments.

Author contributions

S.-J. Lin designed and performed the experiments and data analysis and prepared the manuscript; P.-H. Chao and S.-J. Lin conducted bacteria culture and data analysis and revised the manuscript; H.-W. Cheng provided the SERS substrate and assisted with Raman measurement; Y.-Y. Han assisted in data analysis and wrote the manuscript; J.-K. Wang and Y.-L. Wang provided suggestions for the experiments and the interpretation of data; N.-T. Huang proposed the original idea, guided the experiments, and wrote the manuscript.

Conflicts of interest

The authors declare no conflict of interest. The founding sponsors had no role in the experimental design, in the collection, analyses, and interpretation of data, in the manuscript writing, and in the decision to publish the results.

Acknowledgements

This work was supported by the Ministry of Science and Technology, Taiwan under the grant “MOST 110-2221-E-002-009-MY3” and “MOST 109-2639-M-001-005-ASP”. We are thankful to Dr. Jun-Yi Chien for providing AMP-resistance transfected *E. coli*.

References

- 1 C. J. L. Murray, K. S. Ikuta, F. Sharara, L. Swetschinski, G. Robles Aguilar, A. Gray, C. Han, C. Bisignano, P. Rao, E. Wool, S. C. Johnson, A. J. Browne, M. G. Chipeta, F. Fell, S. Hackett, G. Haines-Woodhouse, B. H. Kashef Hamadani, E. A. P. Kumaran, B. McManigal, R. Agarwal, S. Akech, S. Albertson, J. Amuasi, J. Andrews, A. Aravkin, E. Ashley, F. Bailey, S. Baker, B. Basnyat, A. Bekker, R. Bender, A. Bethou, J. Bielicki, S. Boonkasidecha, J. Bukosia, C. Carvalheiro, C. Castañeda-Orjuela, V. Chansamouth, S. Chaurasia, S. Chiurchiù, F. Chowdhury, A. J. Cook, B. Cooper, T. R. Cressey, E. Criollo-Mora, M. Cunningham, S. Darboe, N. P. J. Day, M. De Luca, K. Dokova, A. Dramowski, S. J. Dunachie, T. Eckmanns, D. Eibach, A. Emami, N. Feasey, N. Fisher-Pearson, K. Forrest, D. Garrett, P. Gastmeier, A. Z. Giref, R. C. Greer, V. Gupta, S. Haller, A. Haselbeck, S. I. Hay, M. Holm, S. Hopkins, K. C. Iregbu, J. Jacobs, D. Jarovsky, F. Javanmardi, M. Khorana, N. Kissoon, E. Kobeissi, T. Kostyanev, F. Krapp, R. Krumkamp, A. Kumar, H. H. Kyu, C. Lim, D. Limmathurotsakul, M. J. Loftus, M. Lunn, J. Ma, N. Mturi, T. Munera-Huertas, P. Musicha, M. M. Mussi-Pinhata, T. Nakamura, R. Nanavati, S. Nangia, P. Newton, C. Ngoun, A. Novotney, D. Nwakanma, C. W. Obiero, A. Olivas-Martinez, P. Olliaro, E. Ooko, E. Ortiz-Brizuela, A. Y. Peleg, C. Perrone, N. Plakkal, A. Ponce-de-Leon, M. Raad, T. Ramdin, A. Riddell, T. Roberts, J. V. Robotham, A. Roca, K. E. Rudd, N. Russell, J. Schnall, J. A. G. Scott, M. Shivamallappa, J. Sifuentes-Osornio, N. Steenkeste, A. J. Stewardson, T. Stoeva, N. Tasak, A. Thaiprakong, G. Thwaites, C. Turner, P. Turner, H. R. van Doorn, S. Velaphi, A. Vongpradith, H. Vu, T. Walsh, S. Waner, T. Wangrangsimakul, T. Wozniak, P. Zheng, B. Sartorius, A. D. Lopez, A. Stergachis, C. Moore, C. Dolecek and M. Naghavi, *Lancet*, 2022, **399**, 629–655.
- 2 K.-D. Vihta, N. C. Gordon, N. Stoesser, T. P. Quan, C. S. B. Tyrrell, M. Vongsouvath, E. A. Ashley, V. Chansamouth, P. Turner, C. L. Ling, D. W. Eyre, N. J. White, D. Crook, T. E. A. Peto and A. S. Walker, *Sci. Rep.*, 2021, **11**, 23359.
- 3 M. S. Bader, M. Loeb, D. Leto and A. A. Brooks, *Postgrad. Med.*, 2020, **132**, 234–250.
- 4 M. P. Weinstein, Methods for Dilution Antimicrobial Susceptibility Tests for Bacteria that Grow Aerobically,

- National Committee for Clinical Laboratory Standards, 2018.
- 5 I. Wiegand, K. Hilpert and R. E. W. Hancock, *Nat. Protoc.*, 2008, **3**, 163–175.
 - 6 M. C. F. van Teeseling, M. A. de Pedro and F. Cava, *Front. Microbiol.*, 2017, **8**, 1264.
 - 7 T. Zahir, R. Camacho, R. Vitale, C. Ruckebusch, J. Hofkens, M. Fauvert and J. Michiels, *Commun. Biol.*, 2019, **2**, 269.
 - 8 M. Sinha, J. Jupe, H. Mack, T. P. Coleman, S. M. Lawrence and S. I. Fraley, *Clin. Microbiol. Rev.*, 2018, **31**, e00089-17.
 - 9 L. Samuel, *J. Appl. Lab. Med.*, 2019, **3**, 631–642.
 - 10 G. B. Rogers, P. Marsh, A. F. Stressmann, C. E. Allen, T. V. W. Daniels, M. P. Carroll and K. D. Bruce, *Clin. Microbiol. Infect.*, 2010, **16**, 1656–1658.
 - 11 O. Opota, K. Jaton and G. Greub, *Clin. Microbiol. Infect.*, 2015, **21**, 323–331.
 - 12 C. Y. Liu, Y. Y. Han, P. H. Shih, W. N. Lian, H. H. Wang, C. H. Lin, P. R. Hsueh, J. K. Wang and Y. L. Wang, *Sci. Rep.*, 2016, **6**, 23375.
 - 13 Y.-Y. Han, Y.-C. Lin, W.-C. Cheng, Y.-T. Lin, L.-J. Teng, J.-K. Wang and Y.-L. Wang, *Sci. Rep.*, 2020, **10**, 12538.
 - 14 H. Shi, Z. Hou, Y. Zhao, K. Nie, B. Dong, L. Chao, S. Shang, M. Long and Z. Liu, *Chem. Eng. J.*, 2019, **359**, 1327–1338.
 - 15 F. E. Chen, A. Kaushik, K. Hsieh, E. Chang, L. Chen, P. Zhang and T. H. Wang, *Anal. Chem.*, 2021, **93**, 1260–1265.
 - 16 M. Azizi, B. Davaji, A. V. Nguyen, A. Mokhtare, S. Zhang, B. Dogan, P. A. Gibney, K. W. Simpson and A. Abbaspourrad, *Biosens. Bioelectron.*, 2021, **178**, 113038.
 - 17 J. He, X. Mu, Z. Guo, H. Hao, C. Zhang, Z. Zhao and Q. Wang, *Eur. J. Clin. Microbiol. Infect. Dis.*, 2014, **33**, 2223–2230.
 - 18 S. C. Kim, S. Cestellos-Blanco, K. Inoue and R. N. Zare, *Antibiotics*, 2015, **4**, 455–466.
 - 19 H. Sun, C. W. Chan, Y. Wang, X. Yao, X. Mu, X. Lu, J. Zhou, Z. Cai and K. Ren, *Lab Chip*, 2019, **19**, 2915–2924.
 - 20 H. Somaweera, A. Ibragimov and D. Pappas, *Analyst*, 2013, **138**, 5566–5571.
 - 21 H. Somaweera, S. O. Haputhanthri, A. Ibragimov and D. Pappas, *Analyst*, 2015, **140**, 5029–5038.
 - 22 M. Azizi, B. Davaji, A. V. Nguyen, S. Zhang, B. Dogan, K. W. Simpson and A. Abbaspourrad, *ACS Sens.*, 2021, **6**, 1560–1571.
 - 23 A. V. Nguyen, M. Azizi, M. Yaghoobi, B. Dogan, S. Zhang, K. W. Simpson and A. Abbaspourrad, *Anal. Chem.*, 2021, **93**, 5789–5796.
 - 24 K. Kim, S. Kim and J. S. Jeon, *Sensors*, 2018, **18**(2), 447.
 - 25 S. Kim, S. Lee, J. K. Kim, H. J. Chung and J. S. Jeon, *Biomicrofluidics*, 2019, **13**, 014108.
 - 26 S. Kim, F. Masum, J. K. Kim, H. J. Chung and J. S. Jeon, *Lab Chip*, 2019, **19**, 959–973.
 - 27 M. Kalashnikov, M. Mueller, C. McBeth, J. C. Lee, J. Campbell, A. Sharon and A. F. Sauer-Budge, *Sci. Rep.*, 2017, **7**, 8031.
 - 28 J. Kirchhoff, U. Glaser, J. A. Bohnert, M. W. Pletz, J. Popp and U. Neugebauer, *Anal. Chem.*, 2018, **90**, 1811–1818.
 - 29 H.-K. Huang, H.-W. Cheng, C.-C. Liao, S.-J. Lin, Y.-Z. Chen, J.-K. Wang, Y.-L. Wang and N.-T. Huang, *Lab Chip*, 2020, **20**, 2520–2528.
 - 30 W. R. Premasiri, J. C. Lee, A. Sauer-Budge, R. Théberge, C. E. Costello and L. D. Ziegler, *Anal. Bioanal. Chem.*, 2016, **408**, 4631–4647.
 - 31 S. W.-Y. Chiu, H.-W. Cheng, Z.-X. Chen, H.-H. Wang, M.-Y. Lai, J.-K. Wang and Y.-L. Wang, *Phys. Chem. Chem. Phys.*, 2018, **20**, 8032–8041.
 - 32 K.-W. Chang, H.-W. Cheng, J. Shiue, J.-K. Wang, Y.-L. Wang and N.-T. Huang, *Anal. Chem.*, 2019, **91**, 10988–10995.
 - 33 M. Morháč and V. Matoušek, *Appl. Spectrosc.*, 2008, **62**, 91–106.
 - 34 C.-C. Liao, Y.-Z. Chen, S.-J. Lin, H.-W. Cheng, J.-K. Wang, Y.-L. Wang, Y.-Y. Han and N.-T. Huang, *Biosens. Bioelectron.*, 2021, **191**, 113483.
 - 35 S. Waśik, M. Arabski, Z. Drulis-Kawa and J. Gubernator, *Eur. Biophys. J.*, 2013, **42**, 549–558.
 - 36 A. Stebbing, *Sci. Total Environ.*, 1982, **22**, 213–234.